Available online at www.sciencedirect.com
ScienceDirect
Gondwana Research 13 (2008) 288–301
www.elsevier.com/locate/gr

Obduction-type granites within the NE Jiangxi Ophiolite: Implications for the final amalgamation between the Yangtze and Cathaysia Blocks

Wu-Xian Li [a], Xian-Hua Li [b,*], Zheng-Xiang Li [c], Fa-Sheng Lou [d]

[a] Key Laboratory of Isotope Geochronology and Geochemistry, Guangzhou Institute of Geochemistry, Chinese Academy of Sciences, Guangzhou 510640, China
[b] State Key Laboratory of Lithospheric Evolution, Institute of Geology and Geophysics, Chinese Academy of Sciences, PO Box 9825, Beijing 100029, China
[c] Institute of Geoscience Research, Department of Applied Geology, Curtin University of Technology, GPO Box U1987, Perth, WA 6845, Australia
[d] Geological Survey of Jiangxi Province, Nanchang 330201, China

Received 29 August 2007; received in revised form 19 December 2007; accepted 24 December 2007
Available online 15 January 2008

Abstract

Leucogranitic lenses are found within the Xiwan ophiolitic mélange in northeastern Jiangxi Province, South China. The leucogranites occur exclusively within the serpentinized peridotite unit of the ophiolite suite. SHRIMP U–Pb zircon dating results indicate that these granites were formed at 880±19 Ma, and were overprinted by an Indosinian tectono-thermal event at ~ 230 Ma. The leucogranites are peraluminous (A/CNK=1.0–1.24), characterized by high Al_2O_3 (14–18.33%) and Na_2O (6.5–10%) and clearly low εNd(T) values of 0.8 to −3.9 compared with the other rock units of the ophiolite suite. On the basis of their REE characters, the leucogranites can be divided into three groups. Group I leucogranites show the most fractionated LREE-enrichment patterns (with La_N/Yb_N and La_N/Sm_N ratios of 30.1–75.0 and 2.3–3.9, respectively). Group II leucogranites have moderately fractionated LREE-enrichment patterns (with La_N/Yb_N and La_N/Sm_N ratios of 13.1–26.5 and 0.8–1.9, respectively). Group III leucogranites are characterized by obviously low total REE contents and flat REE patterns with significant positive Eu anomalies, probably due to small degrees of partial melting. All these leucogranites were likely formed by partial melting of sedimentary rocks from a marginal basin at the Yangtze side of the orogen, beneath a major thrust fault during the obduction of the ophiolite onto the continental crust. They are broadly similar to obduction-related granites within ophiolites identified in many places worldwide. Identification of the ca. 880 Ma obduction-type granites in the NE Jiangxi ophiolite provides a petrological constraint on the timing of the ophiolite obduction onto the continental crust. In combination with the termination of the Shuangxiwu arc magmatism at ca. 890 Ma, we interpret that the close of the Neoproterozoic back-arc basin and the termination of the continental amalgamation between the Yangtze and Cathaysia Blocks occurred at ca. 880 Ma.

Keywords: Granites; Obduction; Ophiolite; Neoproterozoic; South China

1. Introduction

Ophiolites as on-land slices of oceanic lithosphere are important for the study of orogenic evolution and composition of oceanic crust, and for reconstructing ancient continental plate boundaries (e.g. Khan et al., 2007; Dilek et al., 2007; Ishikawa et al., 2007; Zoheir and Klemm, 2007). Most ophiolites are associated with volumetrically minor granitic rocks that are often called plagiogranites, traditionally thought to be the end products of either high differentiation of basaltic magma, or partial melting of altered oceanic basaltic rocks in high temperature shear zones close to a spreading center (e.g., Coleman and Peterman, 1975; Coleman and Donato, 1979; Aldiss, 1981; Pedersen and Malpas, 1984; Flagler and Spray, 1991). However, more recent studies demonstrate that some granitic rocks within ophiolite suites can also be formed by partial melting of either the subducted slab (e.g., Sorenson and Grossman, 1989; Li and Li, 2003; Yoshikawa and Ozawa, 2007) or marginal-basin sedimentary rocks beneath major thrust faults during the obduction of ophiolites onto the continental crust (e.g., Pearce, 1989; Cox et al., 1999). Thus, the granitic rocks within ophiolite

* Corresponding author. Previously at the Guangzhou Institute of Geochemistry, Chinese Academy of Sciences, PR China. Tel.: +86 10 62007395; fax: +86 10 62010846.
E-mail address: lixh@gig.ac.cn (X.-H. Li).

1342-937X/$ - see front matter © 2007 International Association for Gondwana Research. Published by Elsevier B.V. All rights reserved.
doi:10.1016/j.gr.2007.12.010

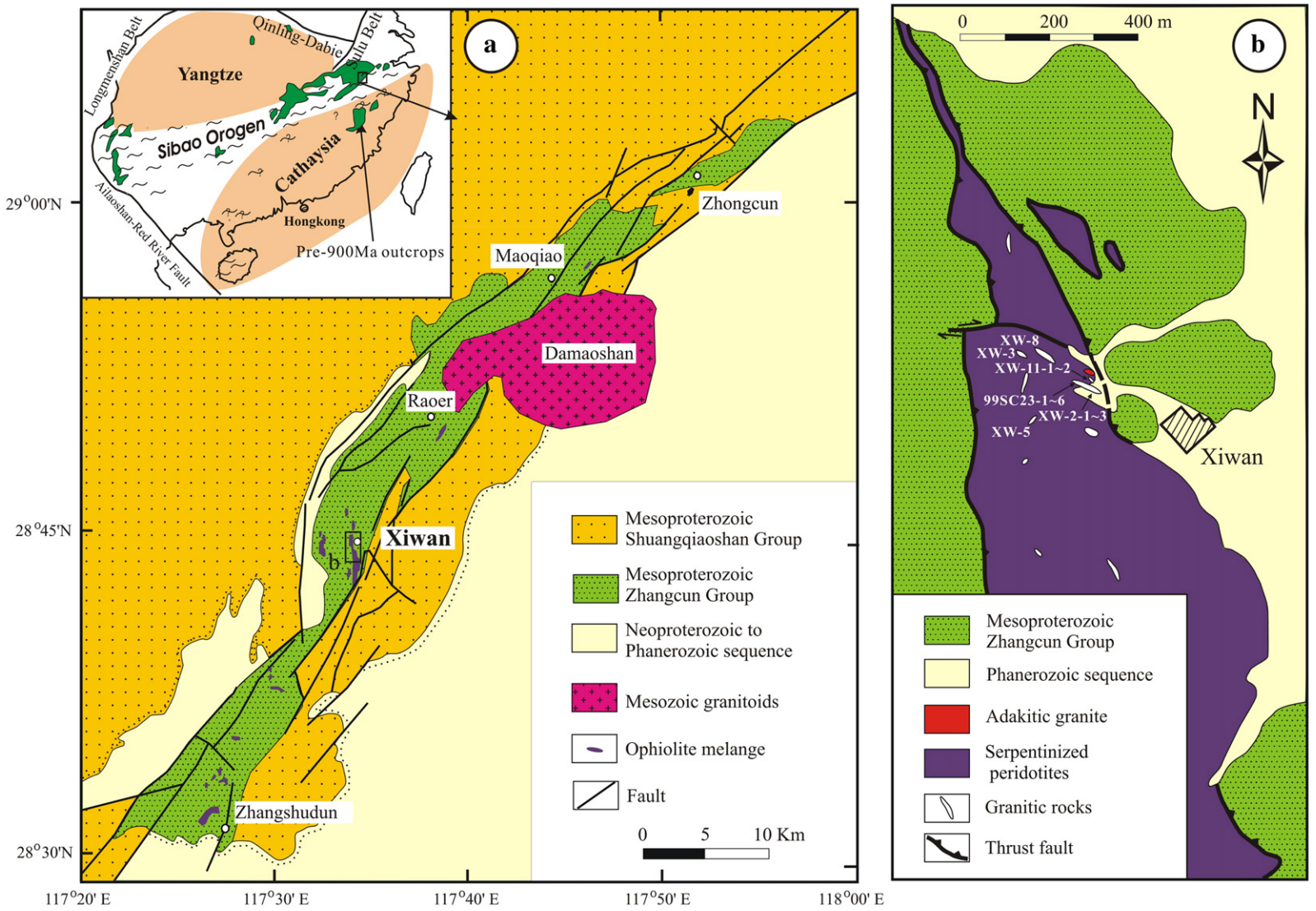

Fig. 1. (a) A simplified geological map of the NE Jiangxi ophiolite mélange; Insert shows the Pre-900 Ma outcrops in South China. (b) The distribution of leucogranitic (white) and adakitic (red) lenses within the serpentinized peridotite of the Xiwan ophiolitic mélange. (For interpretation of the references to colour in this figure legend, the reader is referred to the web version of this article.)

suites can be subdivided into four types in a more general classification scheme, i.e. the fractionation-type and the shear-type generated during sea-floor spreading, and the subduction and obduction types formed during the subduction or obduction of oceanic crust, respectively (Li and Li, 2003). Consequently, dating these different types of granitic rocks within ophiolite suites would provide important time constrains on key events of oceanic crustal evolution during the Wilson cycle.

Obduction-type granitic rocks have previously been found in numerous places worldwide, such as in the northern Semail ophiolite of the United Arab Emirates (Cox et al., 1999), the Guevgueli ophiolitic complex of the Greek Macedonia (Pearce, 1989), the Lizard ophiolitic complex of SW England (Pearce, 1989), and the Thetford Mines ophiolite of the Canadian Appalachians (Whitehead et al., 2000). In the northern Semail ophiolite, Sm–Nd isochron dating of the granites yielded an age of 98.8±9.5 Ma, consistent with the metamorphic age (~ 95 Ma) of the amphibolite-facies metamorphic sole beneath the thrust sheet (Hacker, 1994; Hacker et al., 1996), confirming that the age of the obduction-related granites could represent the emplacement time of the ophiolite onto the continent.

The South China Block is generally believed to have been formed through the amalgamation of the Yangtze and Cathaysia Blocks during the Sibao orogeny. However, the timing and evolution of the Sibao orogeny are highly controversial, with most researchers preferring either a ca. 1.1–0.90 Ga age (e.g., Li et al., 2002a, 2006, 2007a; Li and Li, 2003; Ye et al., 2007) or ages as young as ca. 0.8 Ga (Li, 1999; Zhou et al., 2002a,b; 2006a,b; Wang et al., 2007). We report in this paper SHRIMP zircon U-Pb geochronology, geochemistry and Nd isotopes of leucogranitic lenses from the Xiwan ophiolitic mélange in northeastern Jiangxi Province. Our results demonstrate that these leucogranitic rocks were obduction-related. These results have significant implications for the evolution of the NE Jiangxi ophiolite and constrain the timing of the final amalgamation between the Yangtze and Cathaysia Blocks.

2. Geological background and petrography

The South China Block is bounded by the Qinling-Dabie-Sulu orogenic belt to the north, the Longmenshan Fault to the northwest, and the Ailaoshan-Red River Fault to the southwest (Fig. 1). Pre-900 Ma rocks in South China crop out mainly in the Sibao orogen, along with minor exposures in the interiors of the Yangtze and Cathaysia Blocks (Fig. 1). The NE Jiangxi ophiolite is located in the SE margin of the Yangtze Block, spreading a distance of about 100 km. They consist of a suit of mafic–ultramafic blocks that are in structural contact with the Mesoproterozoic (?) Shuangqiaoshan Group. The part of Shuangqiaoshan Group that is in directly contact with the mafic–ultramafic bodies

Table 1
SHRIMP U–Pb zircon data for the Xiwan leucogranites

	U (ppm)	Th (ppm)	Th/U	f_{206}	$^{207}Pb/^{235}U$		$^{206}Pb/^{238}U$		$^{207}Pb/^{206}Pb$		$^{206}Pb/^{238}U$ age		$^{207}Pb/^{206}Pb$ age	
					(±1σ)		(±1σ)		(±1σ)		(Ma) (±1σ)		(Ma) (±1σ)	
1*	563	269	0.49	0.05	1.327	0.038	0.1410	0.0039	0.0683	0.0006	850.4	21.9	877	18
2*	456	9	0.02	0.19	0.636	0.022	0.0733	0.0021	0.0629	0.0009	455.8	12.2	705	32
3	141	88	0.65	0.26	1.370	0.049	0.1340	0.0039	0.0741	0.0013	810.9	21.8	1045	43
4*	175	36	0.21	0.53	0.976	0.039	0.1068	0.0030	0.0663	0.0011	654.0	17.7	815	60
5	552	253	0.47	0.12	1.751	0.051	0.1462	0.0041	0.0869	0.0007	879.7	22.6	1358	17
6*	321	74	0.24	0.14	0.871	0.028	0.0969	0.0027	0.0652	0.0010	596.0	16.0	781	34
7*	461	87	0.19	0.04	0.862	0.027	0.0955	0.0027	0.0654	0.0008	587.8	15.6	787	25
8*	881	61	0.07	0.18	0.726	0.022	0.0834	0.0023	0.0632	0.0006	516.2	13.6	714	23
9*	472	211	0.46	0.13	1.280	0.038	0.1369	0.0038	0.0678	0.0007	826.9	21.4	863	23
10*	458	183	0.41	0.43	0.830	0.028	0.0925	0.0026	0.0651	0.0008	570.5	15.1	778	25
11	235	76	0.33	0.13	3.290	0.112	0.2385	0.0067	0.1001	0.0019	1378.8	34.7	1625	37
12*	374	121	0.33	0.08	1.003	0.031	0.1099	0.0031	0.0662	0.0009	672.0	17.8	813	27
13*	1367	540	0.41	0.98	0.249	0.005	0.0357	0.0003	0.0506	0.0010	225.8	1.7	224.1	46.1
14	209	128	0.63	0.48	8.573	0.146	0.4107	0.0062	0.1514	0.0010	2217.9	28.4	2362	11
15	170	85	0.52	0.33	2.768	0.050	0.2124	0.0032	0.0945	0.0010	1241.4	17.2	1519	19
16	399	384	1.00	0.10	3.848	0.062	0.2619	0.0039	0.1066	0.0005	1499.5	19.6	1741	9
17	156	128	0.85	0.08	9.208	0.147	0.4192	0.0063	0.1593	0.0008	2256.9	28.5	2448	9
18	267	85	0.33	0.16	6.574	0.099	0.3745	0.0056	0.1273	0.0006	2050.4	25.9	2061	8
19	178	113	0.65	0.31	6.313	0.101	0.3676	0.0055	0.1246	0.0008	2018.0	26.0	2023	12
20	446	191	0.44	0.41	3.766	0.075	0.2474	0.0047	0.1104	0.0007	1424.8	24.2	1807	11
21	424	210	0.51	0.10	10.533	0.158	0.4759	0.0071	0.1605	0.0005	2509.2	30.4	2461	5
22	257	94	0.38	0.08	6.324	0.095	0.3609	0.0054	0.1271	0.0005	1986.2	25.2	2058	8
23	285	146	0.53	0.06	6.338	0.101	0.3682	0.0055	0.1248	0.0006	2021.1	25.6	2027	8
24	198	155	0.81	0.08	4.638	0.093	0.2807	0.0056	0.1198	0.0007	1594.8	27.6	1954	10
25	318	234	0.76	0.07	6.119	0.098	0.3512	0.0053	0.1264	0.0006	1940.5	25.4	2048	9
26	344	123	0.37	0.08	8.069	0.121	0.3737	0.0056	0.1566	0.0006	2047.0	25.7	2419	6
27*	283	244	0.89	0.16	1.386	0.044	0.1452	0.0036	0.0692	0.0007	874.2	12.3	906	22
28	159	120	0.78	0.36	5.046	0.121	0.3220	0.0071	0.1136	0.0011	1799.6	34.1	1858	17
29	260	200	0.79	0.21	6.108	0.098	0.3636	0.0055	0.1218	0.0006	1999.2	25.3	1983	9
30	161	85	0.55	0.15	8.500	0.136	0.4120	0.0062	0.1496	0.0008	2224.2	28.1	2341	9

(1) Data in this table were calculated after ^{204}Pb corrections. All errors are in 1σ. (2) Data with asterisk were used in the crystallization age calculation.

was recently renamed the Zhangcun Group by mapping geologists. The Zhangcun Group consists predominantly of volcaniclastic rocks intercalated with basalts formed in a back-arc basin (Li et al., 2003a). It is in structural contact with the Lower Shuangqiaoshan Group (BGMRJP, 1984).

There are dozens of mafic–ultramafic blocks in the NE Jiangxi ophiolitic belt. Amongst them, the Xiwan ultramafic block is the largest which consists dominantly of strongly serpentinized harzburgite and dunite. Glaucophane and crossite were reported at a few locations within the ultramafic block, indicating that the ophiolite experienced high-pressure metamorphism at $P \approx 12$ Kb and $T \approx 300$–400 °C (Zhou, 1989; Shu et al., 1994; Zhou, 1997). A number of granitic lenses, ranging from less than one meter to several tens of meters in dimension are enclosed exclusively within the ultramafic rocks. They were regarded as intrinsic parts of the ophiolite. Amongst the granitic lenses, some are amphibole-bearing albite granties that have highly positive εNd(t) values similar to adakitic granite (Li and Li, 2003). Others are leucogranites (Fig. 1b).

The leucogranites are light gray in color with fine-grained textures (0.1–0.3 mm × 0.2–0.5 mm), consisting of 20–25% quartz, 60–65% plagioclase (albite/oligoclase) and 10–15% K-feldspar, <5% biotite and accessory minerals such as zircon, apatite and Fe–Ti oxides. The rocks are variably altered, with K-feldspar and plagioclase being argillized and biotites being chloritized. Micrographic texture is common, suggesting that either the rocks were crystallized at a relatively shallow level or have undergone Na metasomatism. Quartz grains in the leucogranites show weakly undulatory extinction but no obvious foliation, which are in contrast to the nearby adakitic granites that were strongly deformed (Li and Li, 2003).

3. Analytical methods

Zircons were separated from a leucogranite sample XW2-2 (28°44'30"N; 117°34'37"E) using standard density and magnetic separation techniques. Representative zircon grains were hand-picked under a binocular microscope. Zircon grains, together with zircon standard Temora, were cast in an epoxy mount, which was then polished to section the crystals in half for analysis. Zircons were documented with transmitted and reflected light micrographs as well as cathodoluminescence (CL) images to reveal their internal structures. Measurements of U, Th, and Pb were conducted using the SHRIMP II ion microprobe at the Beijing SHRIMP Center under standard operating conditions (5-scan cycle, 2 nA primary O_2^- beam, mass resolution ca. 5000). U–Th–Pb rations were determined relative to the TEMORA standard zircon with $^{206}Pb/^{238}U = 0.0668$ corresponding to 417 Ma (Black et al., 2003), and the absolute abundances were calibrated to the standard zircon SL13. Analyses of the TEMORA standard zircon were interspersed with those of unknowns, following operating and data processing procedures similar to those described by Williams (1998). Measured compositions were corrected for common Pb using the ^{204}Pb-method, and an average crustal composition (Cumming and Richards, 1975) appropriate to the age of the mineral was assumed. Uncertainties on individual analyses are reported at 1σ level, and mean ages for pooled $^{206}Pb/^{238}U$ results are quoted at 95% confidence level.

Major element oxides and trace elements were determined using a Varian Vista PRO ICP-AES and a Perkin-Elmer Sciex ELAN 6000 ICP-MS, respectively, at the Guangzhou Institute of Geochemistry, Chinese Academy of Sciences. Procedures for

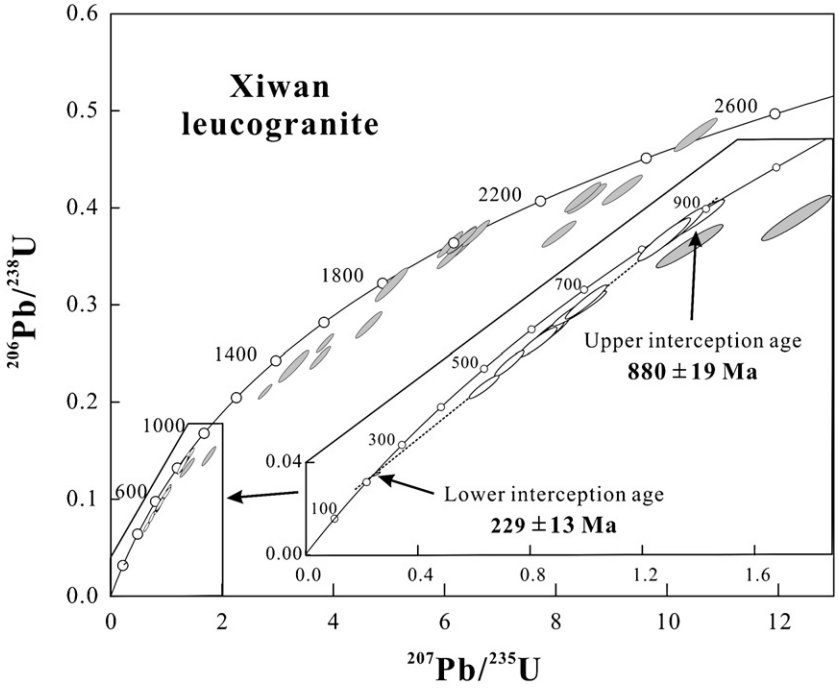

Fig. 2. U–Pb disconcordia diagram showing analytical data for zircons from leucogranites within the Xiwan ophiolitic mélange. Data excluded from age calculation for the sample are shown in gray-filled symbols.

Table 2
Major and trace element data for the Xiwan leucogranites within the NE Jiangxi ophiolite

Sample	XW-11-1	XW-11-2	99SC23-1	99SC23-2	99SC23-3	99SC23-4	99SC23-5
	Group I		Group II				
Major elements (%)							
SiO_2	70.22	72.87	72.23	71.89	69.54	64.06	72.47
TiO_2	0.30	0.23	0.23	0.23	0.25	0.37	0.21
Al_2O_3	16.13	15.88	15.08	15.41	15.51	18.33	14.83
Fe_2O_3	2.43	1.58	1.44	2.16	1.71	3.70	1.26
MnO_2	0.01	0.01	0.01	0.01	0.02	0.01	0.01
MgO	0.87	0.76	0.54	0.93	0.91	2.22	0.58
CaO	0.35	0.30	0.38	0.24	0.63	0.17	0.54
Na_2O	7.38	8.76	7.23	6.53	7.18	8.02	7.33
K_2O	1.66	0.14	1.62	1.91	1.65	1.15	1.20
P_2O_5	0.09	0.11	0.10	0.09	0.07	0.05	0.10
LOI	0.60	0.29	0.89	1.08	1.26	1.54	0.93
Total	99.84	100.83	99.75	100.48	98.73	99.62	99.47
ACNK	1.11	1.05	1.05	1.16	1.05	1.24	1.03
Trace elements (ppm)							
V	15.7	4.62	6.74	10.3	11.6	42.8	9.10
Cr	6.86	8.02	5.91	6.84	8.15	12.9	17.4
Ga	14.8	12.3	15.5	17.2	15.9	22.7	15.0
Ge	0.73	0.62	0.54	0.76	0.60	0.92	0.66
Rb	2.53	0.42	14.7	27.5	17.8	20.1	13.4
Sr	41.9	47.6	261	309	327	288	255
Y	1.77	1.89	13.0	11.9	12.5	14.1	11.3
Zr	204	158	171	173	183	251	153
Nb	22.2	18.5	22.0	22.8	23.0	31.7	19.1
Ba	759	89.8	303	816	486	382	343
La	8.04	15.4	38.2	38.2	41.2	57.0	31.5
Ce	15.7	27.2	70.1	69.6	74.8	90.4	52.5
Pr	1.55	2.40	7.84	7.76	8.48	11.2	6.37
Nd	5.13	7.86	24.5	24.4	27.3	39.4	22.9
Sm	0.75	1.04	3.82	3.80	4.16	6.12	3.74
Eu	0.17	0.26	1.07	0.91	1.12	1.23	0.90
Gd	0.53	0.69	2.68	2.68	2.90	3.20	2.21
Tb	0.07	0.09	0.44	0.41	0.43	0.48	0.36
Dy	0.31	0.35	2.37	2.18	2.26	2.49	2.00
Ho	0.06	0.05	0.43	0.40	0.41	0.48	0.39
Er	0.16	0.14	1.14	1.05	1.12	1.50	1.10
Tm	0.03	0.02	0.18	0.18	0.18	0.25	0.16
Yb	0.19	0.15	1.22	1.23	1.29	1.54	1.03
Lu	0.03	0.02	0.20	0.20	0.22	0.26	0.16
Hf	5.11	3.82	4.24	4.48	4.54	6.40	3.98
Ta	1.86	1.44	1.71	1.90	1.78	2.46	1.43
Th	1.35	1.00	9.35	9.30	9.71	13.2	7.41
U	0.92	1.18	2.49	2.53	2.54	3.47	2.11

Sample	99SC23-6	XW-2-2	XW-2-3	XW-2-1	XW-5	XW-8	XW-3-1
	Group II					Group III	
Major elements (%)							
SiO_2	68.42	70.55	70.95	68.81	69.10	75.03	75.55
TiO_2	0.29	0.28	0.26	0.37	0.22	0.08	0.09
Al_2O_3	19.17	15.59	15.11	15.81	16.06	14.08	13.95
Fe_2O_3	0.53	2.63	2.32	3.69	5.05	1.58	0.87
MnO_2	0.02	0.02	0.02	0.02	0.08	0.01	0.01
MgO	0.11	0.81	0.87	1.76	0.54	0.49	0.58
CaO	0.27	0.37	0.61	0.45	0.32	0.23	0.32
Na_2O	9.95	7.07	7.43	6.74	8.23	8.19	8.13
K_2O	0.14	1.85	1.57	0.97	0.19	0.03	0.04
P_2O_5	0.12	0.10	0.09	0.16	0.01	0.01	0.03
LOI	0.50	0.75	0.80	1.30	0.41	0.33	0.34

Table 2 (*continued*)

Sample	99SC23-6	XW-2-2	XW-2-3	XW-2-1	XW-5	XW-8	XW-3-1
	Group II					Group III	
Total	99.52	99.83	99.83	99.82	99.84	99.90	99.84
ACNK	1.13	1.09	1.01	1.22	1.12	1.01	1.00
Trace elements (ppm)							
V	3.73	19.6	10.2	19.8	8.56	8.16	1.87
Cr	6.15	8.32	7.09	5.35	18.4	6.12	6.58
Ga	16.3	17.5	14.0	15.1	16.4	13.0	10.2
Ge	0.35	0.86	0.68	0.87	0.79	0.05	0.18
Rb	2.20	30.3	6.80	4.49	1.74	1.00	0.23
Sr	347	344	130	103	90.6	28.9	231
Y	14.2	13.1	9.92	6.51	6.91	0.42	0.30
Zr	209	192	190	183	136	31.7	36.3
Nb	26.6	22.7	21.0	18.9	19.1	1.22	1.73
Ba	68.6	864	481	315	850	205	211
La	46.8	42.4	19.5	12.5	18.5	0.66	0.33
Ce	87.1	67.0	39.3	25.4	36.0	1.17	0.68
Pr	9.87	8.29	4.23	2.60	3.52	0.10	0.07
Nd	30.5	29.6	14.8	9.12	10.4	0.30	0.26
Sm	4.72	4.51	2.34	1.46	1.54	0.06	0.05
Eu	1.19	1.07	0.63	0.41	0.31	0.04	0.04
Gd	2.98	2.86	1.83	1.02	1.04	0.05	0.06
Tb	0.48	0.44	0.29	0.18	0.18	0.01	0.01
Dy	2.44	2.32	1.55	0.93	1.10	0.08	0.05
Ho	0.45	0.44	0.31	0.19	0.23	0.02	0.01
Er	1.22	1.29	0.84	0.54	0.71	0.05	0.02
Tm	0.20	0.20	0.14	0.10	0.14	0.01	0.00
Yb	1.36	1.21	0.93	0.64	1.01	0.07	0.03
Lu	0.24	0.20	0.15	0.11	0.18	0.01	0.01
Hf	5.14	4.96	4.54	4.26	3.70	1.33	1.20
Ta	2.06	1.69	1.71	1.43	1.62	0.08	0.11
Th	10.9	10.1	5.69	1.70	10.5	0.36	1.96
U	2.66	2.45	1.72	0.79	2.46	0.12	0.16

major element and trace element analyses were similar to those described by X.H. Li et al. (2000, 2002b). About 40 mg powdered samples were dissolved in platinic crucible using $Li_2B_4O_7+H_3BO_3$ mixture at ca. 1 100 °C for 20 min. For ICP-AES major element analysis, the sample dissolution was spiked with single element In as an internal standard for monitoring the signal drift during measurement, and diluted to a factor of 1/5000. A set of USGS and Chinese national rock standards was chosen for calibrating major element concentration of unknowns. For ICP-MS trace element analysis, an internal standard solution containing the single element Rh was used with a dilution factor of 1/5000. The USGS standards W-2 and GSP-1 were chosen for calibrating element concentrations of measured samples. Analytical precision is 0.5–2% for major elements by ICP-AES, and generally better than 3% for most trace elements by ICP-MS.

Nd fraction was separated by passing through cation columns followed by HDEHP columns. Nd isotopic compositions were determined using a Micromass Isoprobe multi-collector ICPMS (MC-ICPMS) at the Guangzhou Institute of Geochemistry. Samples were taken up in 2% HNO_3, and the aqueous solutions were introduced into the MC-ICPMS using a Meinhard glass nebuliser with an uptake rate of 0.1 mL/min. The inlet system was washed out for 5 min between analyses using high-purity 5% HNO_3 followed by a blank solution of 2% HNO_3 from which the sample solutions were prepared. The Isoprobe MC-ICPMS was

operated in a static mode, and yielded $^{143}Nd/^{144}Nd = 0.512125 \pm 11$ (2σ) on 14 runs for the Shin Etou JNdi-1 standard during this study. Analytical procedures were similar to those described by X.H. Li et al. (2004). Measured $^{143}Nd/^{144}Nd$ ratios were normalized to $^{146}Nd/^{144}Nd = 0.7219$. The reported $^{143}Nd/^{144}Nd$ ratios are adjusted relative to the Shin Etsu JNdi-1 standard of 0.512115, corresponding to the La Jolla standard of 0.511860 (Tanaka et al., 2000).

4. Results

4.1. SHRIMP U–Pb zircon age

The zircons are mostly anhedral and rounded, 20 to 50 μm long, with length to width ratios of 1:1 to 2:1. Most zircons are relatively transparent and colourless, showing magmatic zoning under CL. Thirty analyses of 30 zircons were obtained (Table 1). U concentrations range from 141 to 881 ppm (except for spot 13 of 1367 ppm), Th from 9 to 540 ppm, and Th/U ratios from 0.02 to 1.0. Common Pb is low, the proportion of ^{206}Pb in total measured ^{206}Pb (f_{206} in Table 1) being <1% (Table 1). Most U–Pb zircon data are discordant due to varying degrees of radiogenic Pb loss (Fig. 2). Eleven relatively younger zircons form a discordia line (MSWD = 0.44) with the upper and the lower intercept ages being 880 ± 19 Ma and 229 ± 13 Ma, respectively (Fig. 2). We interpret the upper intercept age of 880 ± 19 Ma as the crystallization age of the leucogranite. The zircons are mostly anhedral and rounded, probably due to formation in high temperature and high pressure followed by up-ward intrusion and rapid crystallization (Corfu et al., 2003). The lower intercept age of 229 ± 13 Ma is interpreted as the timing of the regional Indosinian orogenic overprinting (Li and Li, 2007b). The other zircons have significantly older $^{207}Pb/^{206}Pb$ ages of between 1045 and 2362 Ma, interpreted as either inheritance from the source rocks or xenocryst minerals.

4.2. Geochemistry

Fourteen leucogranite samples from Xiwan were analyzed for major and trace elements (Table 2). All samples are peraluminous, with A/CNK = 1.0–1.24 and variably high Al_2O_3 (14.0–18.3%) and Na_2O (6.5–10.0%). On the basis of their geochemical features, these leucogranites can be subdivided into three groups. Group I samples have moderate SiO_2 contents of between 69% and 73%; Group II leucogranites have the lowest and widest range of SiO_2 contents between 64% and 72.5%; Group III rocks have the highest SiO_2 contents of >75%. In the Harker diagrams (Fig. 3), TiO_2, Al_2O_3, Fe_2O_3, MgO and La of all samples increase with increasing SiO_2, whereas Na_2O, CaO and K_2O are scattered and remain nearly constant. Except for Group III rocks, P_2O_5 increases with increasing SiO_2, showing a S-type granite trend (Chappell, 1999; Li et al., 2007d).

Group I and II leucogranites display fractionated REE patterns (Fig. 4) with small to nil Eu negative anomalies (Eu/Eu* = 0.80–1.0), whereas Group III rocks show nearly flat REE patterns with extremely low REE abundance and pronounced Eu positive anomalies (Eu/Eu* = 2.2–2.4). Group I samples exhibit more LREE-enriched patterns ($La_N/Yb_N = 30.1–75.0$ and $La_N/Sm_N = 2.3–3.9$) than Group II granites ($La_N/Yb_N = 13.1–26.5$ and $La_N/Sm_N = 0.8–1.9$). In the primitive mantle-normalized spidergrams, Group I leucogranites show right-dipping patterns with enrichments in Nb, Ta, Zr and Hf and depletions in Th. Contrarily, Group II leucogranites display "spiky", right-dipping patterns with depletions in Nb, Ta, Sr and P but enrichments in Th, Zr and Hf, except for sample XW-2-1 that is depleted in Th and enriched in P. It is noted that Group III rocks have the lowest abundance of most incompatible trace elements (0.1–10 times of primitive mantle contents). Their trace element patterns are characterized by relative enrichments in Th, Sr, P, Zr, Hf and Ti, similar to those of pegmatites formed by small degrees of partial melting of metasedimentary rocks in the Catalina ophiolitic schist (Sorenson and Grossman, 1989).

Eleven of the 14 samples were analyzed for Nd isotopes (Table 3). Their $^{147}Sm/^{144}Nd$ ratios range from 0.0800 to 0.0985, and the measured $^{143}Nd/^{144}Nd$ ratios from 0.511836 to 0.511975. Calculated initial εNd(T) values are between 0.80 and −3.88. The Nd model ages (T_{DM}) cluster around 1.35–1.65 Ga, suggesting that the granites were derived mainly from a crustal source with Mesoproterozoic residence ages.

5. Discussion

5.1. Petrogenesis

Granitic rocks within ophiolite suites can be grouped into four major genetic types (Li and Li, 2003), i.e., (1) the fractionation-type granites formed by extensive fractional crystallization of oceanic basaltic rocks at high level (Coleman and Peterman, 1975); (2) the shear-type granites generated by anatexis of amphibolites that were metamorphosed from oceanic basaltic rocks within high temperature shear zones in the lower parts of oceanic crust close to a spreading center (Flagler and Spray, 1991); (3) the subduction-type granites formed by dehydration melting of subducted oceanic crust at high pressure with garnet and amphibole as the main residual minerals (Li and Li, 2003); and (4) the obduction-type granties originated from anatexis of sedimentary rocks and/or igneous rocks in marginal basins beneath ophiolite thrust sheets during the obduction of ophiolite onto the continent (Pearce, 1989, Cox et al., 1999).

The Xiwan leucogranites are characterized by peraluminous feature (A/CNK ≥ 1.0) and clearly lower εNd(T) values (0.80 to −3.88) than associated oceanic basaltic rocks (εNd(T) = 4.7 to 8.4) and ca. 0.97 Ga adakitic granites (εNd(T) = 4.9 to 6.7) within the ophiolite complex (Li et al., 1997; Li and Li, 2003). Therefore, these leucogranites are genetically unrelated with the mafic rock units of the ophiolite. Their genesis should thus be different from those of the fractionation-type, the shear-type and the subduction-type granites within ophiolites. On the other hand, their peraluminous nature and low εNd(T) values, as well as the Mesoproterozoic T_{DM} of 1.35–1.65 Ga, are consistent

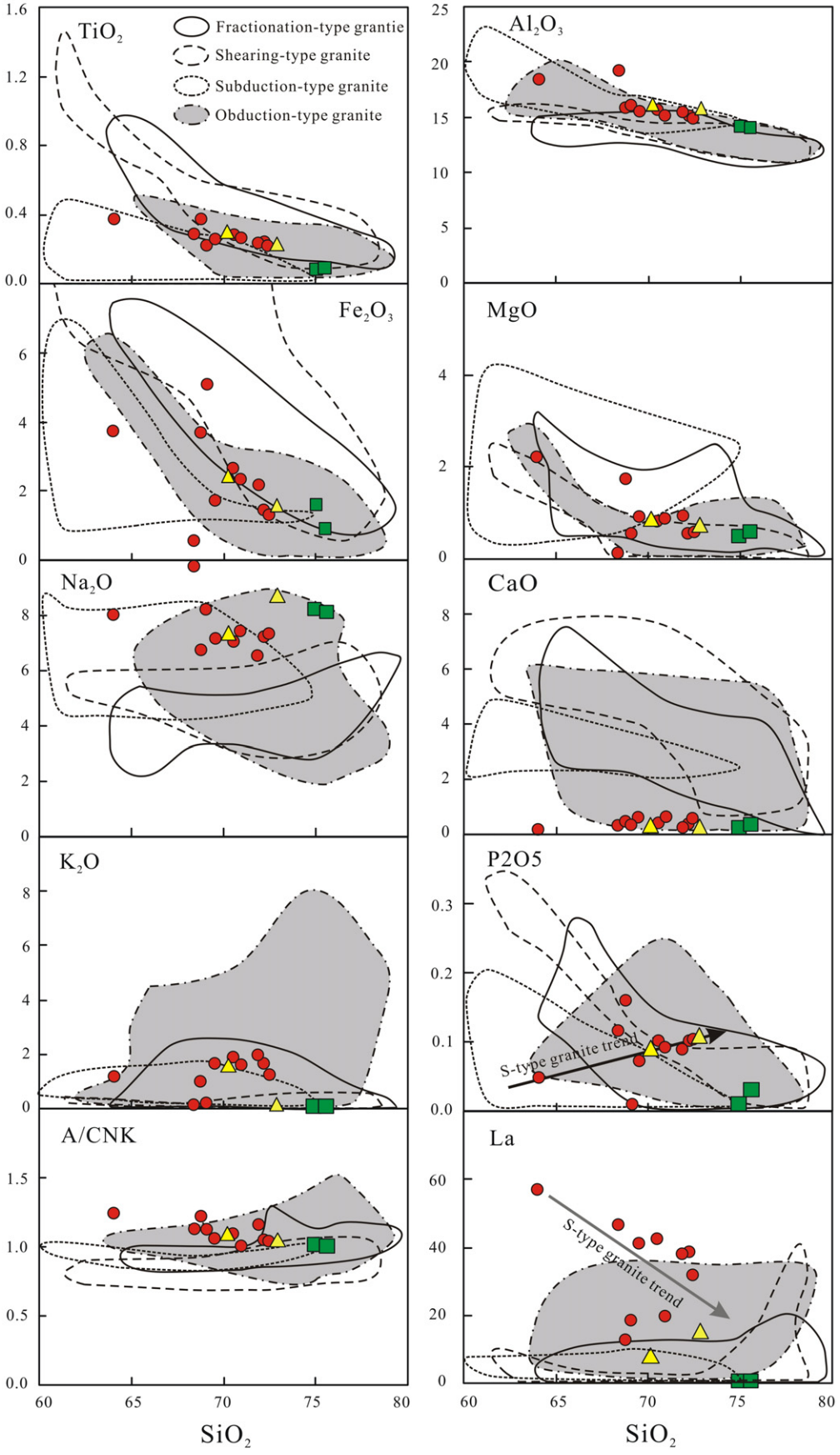
TiO2
Fractionation-type grantie
Shearing-type granite
Subduction-type granite
Obduction-type granite
Al2O3
Fe2O3
MgO
Na2O
CaO
K2O
P2O5
S-type granite trend
A/CNK
La
S-type granite trend
SiO2
SiO2

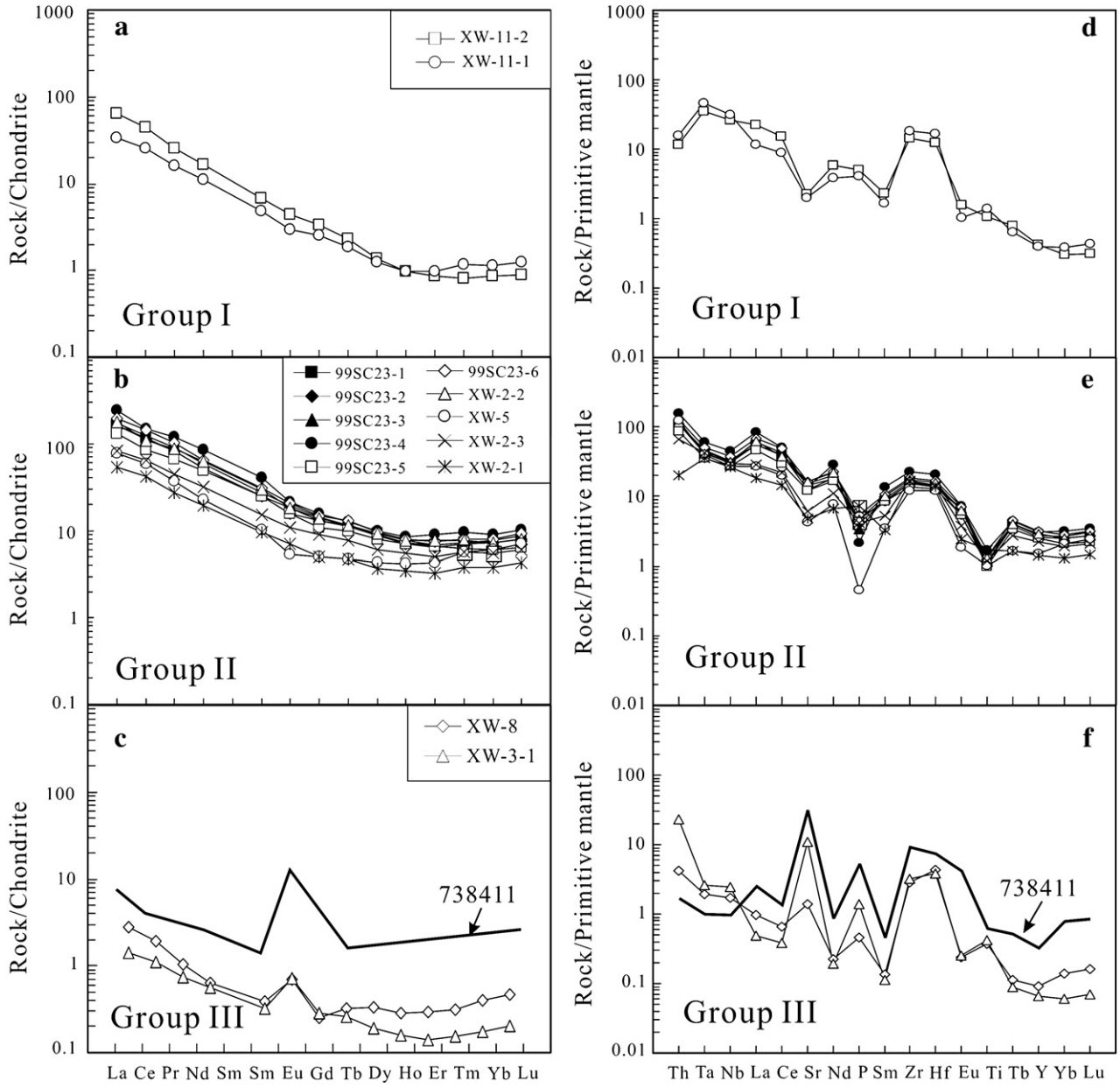

Fig. 4. Chondrite-normalized REE diagrams (a–c) and primitive mantle-normalized trace elements diagrams (d–f) for the three groups of leucogranites. The data of 738411 was from a pegmatite dyke in the metasedimentary rocks of the Catalina ophiolitic schist (Sorenson and Grossman, 1989). Normalization values are from Sun and McDonough (1989).

with their derivation from continental crustal sources. It is noted that the Xiwan leucogranites are geochemically and Nd isotopically similar to those of the Mesoproterozoic metasedimentary rock and adjacent Neoproterozoic peraluminous granites (Li et al., 2003b; Wu et al., 2006). Overall, they share geochemical characteristics with the obduction-type granites (Fig. 3). Several other lines of evidence also support the Xiwan leucogranites being obduction-type granites formed by partial melting of marginal basin sedimentary rocks beneath the major fault zone during the obduction of the ophiolite onto the Yangtze Block. (1) Their formation age of ca. 880 Ma is significantly younger than the ca. 1000 Ma rock age for the ophiolite (Chen et al., 1991). (2) The leucogranites occur exclusively as lenses in the serpentinized mantle peridotite, but

Fig. 3. Harker SiO_2 variation diagrams of the Xiwan leucogranites in comparison with fractionation-type granites (data after Coleman, 1977; Coleman and Donato, 1979; Dixon and Rutherford, 1979; Elthon, 1991; Whitehead et al., 2000; Ahmed, 2003), shear-type granites (data after Pedersen and Malpas, 1984; Flagler and Spray, 1991), subduction-type granites (data after Li and Li, 2003; Liu et al., 2003; Ahmed, 2003) and obduction-type granites (data after Pearce, 1989; Peter and Kamber, 1994; Cox et al., 1999; Skjerlie et al., 2000; Whitehead et al., 2000). Yellow triangle=Group I leucogranite; Red circle=Group II leucogranite; Green square=Group III leucogranite. (For interpretation of the references to colour in this figure legend, the reader is referred to the web version of this article.)

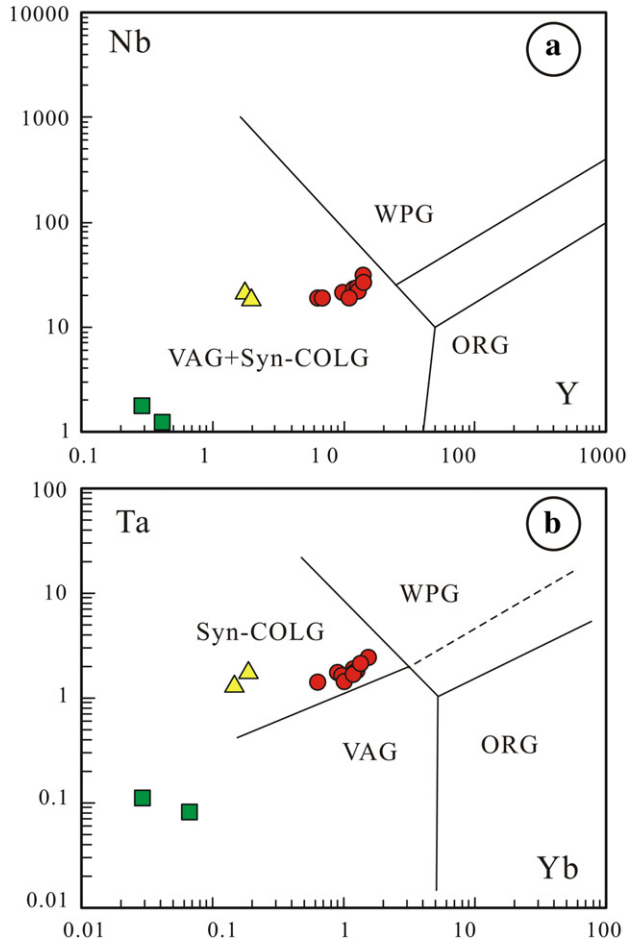

Fig. 5. Geochemical discrimination diagrams of Nb–Y (a) and Ta–Yb (b) for the Xiwan leucogranites (after Pearce et al., 1984), showing the fields of volcanic-arc granites (VAG), syn-collisional granites (syn-COLG), within-plate granites (WPG) and ocean-ridge granites (ORG).

not in the crustal units of the ophiolite (i.e. the basalt and gabbro units). (3) In the Nb vs. Y and Ta vs. Yb diagrams (Fig. 5) of Pearce et al. (1984), the granites plot exclusively into the field of

Table 3
Nd isotopic data for the Xiwan leucogranites within NE Jiangxi ophiolite

Sample	Sm (ppm)	Nd (ppm)	$^{147}Sm/^{144}Nd$	$^{143}Nd/^{144}Nd$	$\pm 2\sigma_m$	T_{DM} (Ga)	εNd(T)
XW-11-1	0.75	5.13	0.0879	0.511967	0.000009	1.43	−0.84
XW-11-2	1.04	7.86	0.0800	0.511904	0.000012	1.42	−1.18
99SC23-1	3.82	24.52	0.0943	0.511939	0.000011	1.55	−2.11
99SC23-2	3.80	24.36	0.0942	0.511975	0.000010	1.50	−1.40
99SC23-3	4.16	27.25	0.0924	0.511974	0.000012	1.48	−1.22
99SC23-4	6.12	39.37	0.0940	0.512071	0.000011	1.37	0.51
99SC23-5	3.74	22.94	0.0985	0.512076	0.000012	1.42	0.09
99SC23-6	4.72	30.45	0.0938	0.512085	0.000011	1.35	0.80
XW-2-2	4.51	29.63	0.0921	0.511836	0.000010	1.65	−3.88
XW-2-3	2.34	14.81	0.0956	0.511887	0.000009	1.63	−3.27
XW-2-1	1.46	9.12	0.0968	0.511939	0.000010	1.58	−2.39

T=880 Ma, the crystallization age of the leucogranites.

syn-collision granite. (4) The abundance of fine-grained, 1045–2362 Ma zircons in the leucogranites reflects inheritance from sedimentary sources.

The three groups of the Xiwan lecuogranites display clearly different geochemical features, particularly different REE patterns, likely reflecting partial melt of sedimentary rocks at different conditions during the obduction of the ophiolite (Fig. 6). Group I leucogranites have the highest La_N/Yb_N (30.1–75.0) and obviously positive Zr and Hf anomalies (Fig. 4), suggesting that they were likely formed at relatively deep positions with garnet being a residual mineral (>10 kb) (Drummond and Defant, 1990; Patiño Douce and Harris, 1998). Group II leucogranites have moderate La/Yb_N of 13.1 to 26.5, indicating that they were formed at relatively shallower depth above the garnet stability field (<10 kb). Group III granites are extremely low in total REE concentrations and have pronounced positive Eu anomalies, pointing to a smaller degree of partial melting of sedimentary rocks similar to the pegmatites within the Catalina ophiolitic Schist (sample 738411, Sorenson and Grossman, 1989).

We note that the Xiwan leucogranites have very high Na_2O contents (6.53–9.95%), suggesting that the leucogranites were formed at either relatively high pressures of >10 kb (Patiño Douce and Harris, 1998) or H_2O-flux melt conditions that

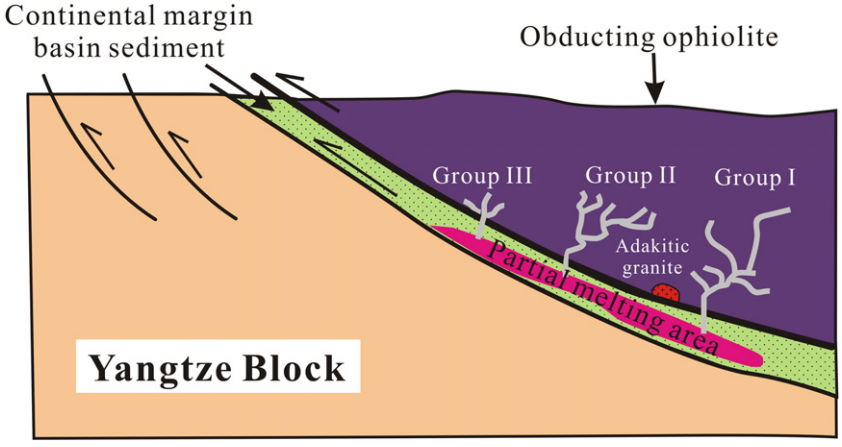

Fig. 6. A tectonic model for the generation and emplacement of the Xiwan obduction-type leucogranites (modified from Cox et al., 1999).

produced a higher proportion of residue alkali feldspar in the source (Patiño Douce and Harris, 1998; Patiño Douce and McCarthy, 1998), or the sedimentary source rocks were metasomatized by Na-enriched sea-water. Three groups of the leucogranites are characteristically high in Na_2O contents and show flat correlation trends in the Na_2O vs. SiO_2 diagrams (Fig. 3), suggesting that Na-enrichment of the leucogranites were likely caused by H_2O-fluxed melting conditions and abnormally Na-enriched sedimentary source rocks, rather than by higher pressure.

5.2. Provenance of the sedimentary protolith

Determination of the provenance of the sedimentary protolith for the Xiwan leucogranites will help to understand the tectonic evolution of Neoproterozoic SE Yangtze Block. Fig. 7 is a cumulative probability plot of $^{207}Pb/^{206}Pb$ age for 19 inherited zircons from the Xiwan leucogranites and two histogram distribution diagrams of magmatic and metamorphic zircon ages from the basement rocks (Pre-900 Ma) of Yangtze and Cathaysia Blocks. These inherited zircon ages cluster at two populations of 2300–2500 Ma (5 spots) and 1700–2100 Ma (10 spots), with four just below 1700 Ma. These zircon ages are inconsistent with crustal ages of the Cathaysia Block that has shown no >1900 Ma magmatic and metamorphic events, but are consistent with those of the Yangtze Block. The absence of Archean-aged zircon in the Xiwan leucogranites is probably due to the low number of analyzed spots. The presence of only a few Sibao-aged (1300–900 Ma) zircons (3 grains) within a dominantly Yangtze-affinitive zircon population suggests that the sedimentary rocks came from a passive continental margin basin near the Yangtze Block (Fig. 8), rather than a Sibaoian foreland basin which should contain a relatively large proportion of Sibao-aged zircons. We interpret that the newborn back-arc basin dividing the Yangtze-side continental margin and the Sibaoian Shuangxiwu arc prevented more Sibao-aged zircons

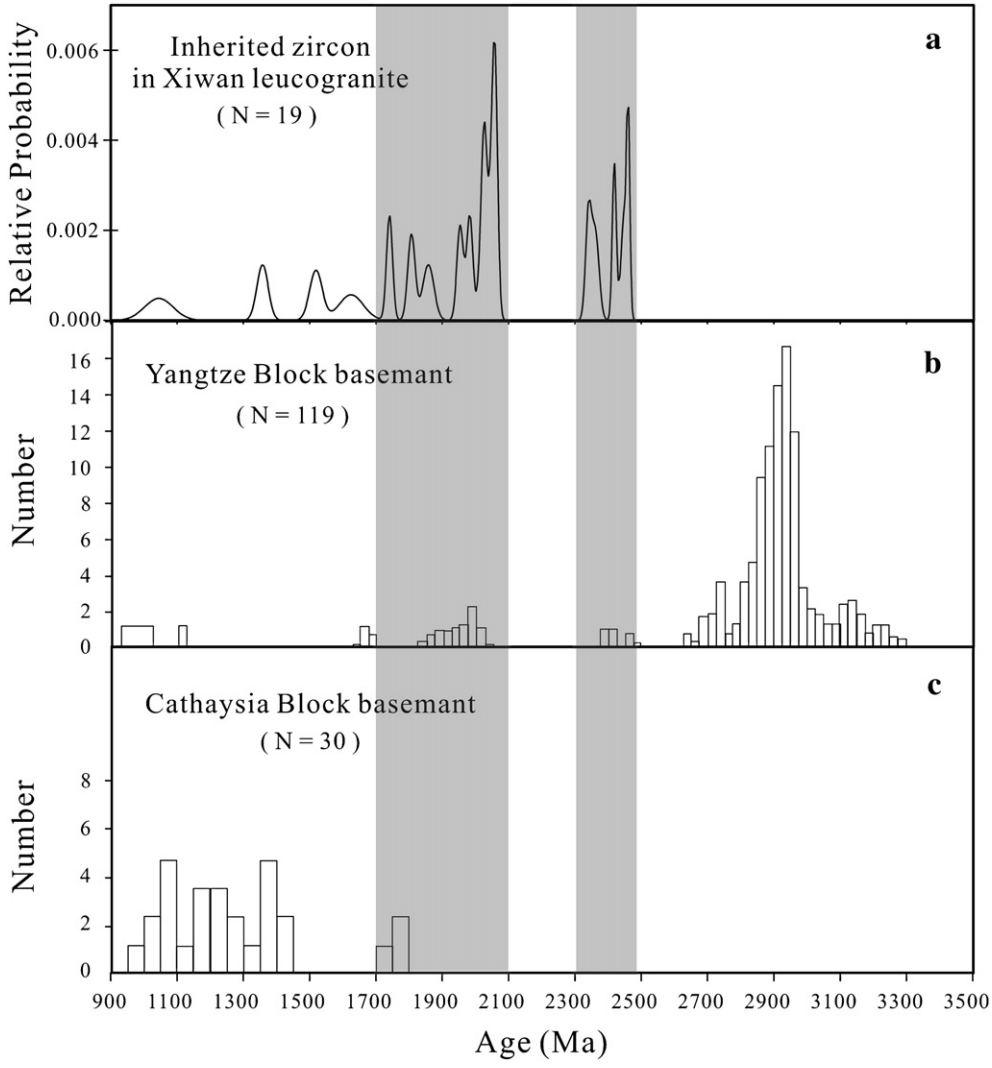

Fig. 7. Cumulative probability plot of inherited zircon $^{207}Pb/^{206}Pb$ ages from Xiwan leucogranites (a) and histogram distribution of magmatic and metamorphic zircon ages from the Pre-900 Ma basement rocks of (b) the Yangtze Block (Hu et al., 1991; Qiu et al., 2000; Zhang et al., 2006; Greentree et al., 2006) and (c) the Cathaysia Block (Li, 1997; Li et al., 2002a,c).

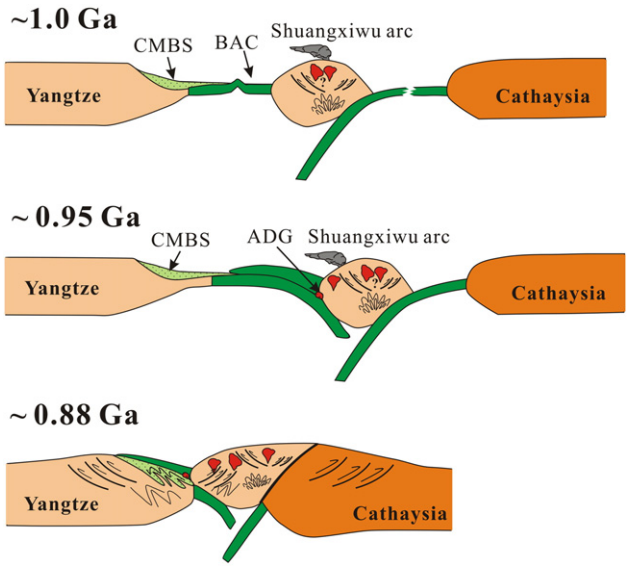

Fig. 8. A cartoon diagram showing tectonic evolution of the SE Yangtze Block during ca. 1.0 to 0.88 Ga (see text for detailed discussions). BAC — back-arc basin; CMBS — continental marginal basin sedimentary rocks; ADK — adakitic granites.

from being deposited on the Yangtze side (Fig. 8). Our work suggests that the back-arc basin closed by the obduction of the Shuangxiwu arc/active continental margin onto the Yangtze Block, which is contrary to the model proposed by Charvet et al. (1996).

5.3. Tectonic evolution of SE Yangtze Block during early Neoproterozoic

We use Fig. 8 to illustrate a tectonic model for SE Yangtze Block between ca. 1.1 Ga and 0.88 Ga, taking into account available geological, geochronological and geochemical data. (1) 1042–1015 Ma Ar–Ar ages of white mica in the Tianli Schists suggest the presence of northward subduction along the early Shuangxiwu arc, SE of the Yangtze Block (Li et al., 2007a). A back-arc basin likely developed behind the active continental margin as evidenced by the 1034±24 Ma ophiolite in NE Jiangxi Province (Chen et al., 1991); (2) The 966±4 Ma white mica Ar–Ar age from the Tianli Schists and the 968±23 Ma adakitic granite within the NE-Jiangxi ophiolite suggest subduction of the back-arc basin toward the Shuangxiwu arc (Li et al., 2007a). (3) The magmatic activities in the Shuangxiwu arc lasted until ca. 900 Ma (Cheng, 1991, 1993; Ye et al., 2007); (4) The 880±19 Ma obduction-type granites within the NE Jiangxi ophiolite suggest the final close of the back-arc basin and amalgamation between the Yangtze and Cathaysia Blocks at ~ 880 Ma.

5.4. Broader tectonic implications

Meso- to Neoproterozoic tectonic evolution of South China has been an issue of hot debate. A key controversy is the timing of the Sibao orogeny, with two major competing viewpoints. One is that the orogenesis between the Yangtze and Cathaysia Blocks did not complete until ca. 0.8 Ga or even younger, and the vast amount of Neoproterozoic (830–750 Ma) magmatism were related to the subduction and/or continental collision (e.g., X.H. Li, 1999; Zhou et al., 2002a,b; Wang et al., 2004; Zhou et al., 2006a,b; Wang et al., 2006). Consequently, the Yangtze Block would have to be an isolated continent surrounded by oceanic subduction (Zhou et al., 2002a) during Rodinian time (>900 Ma to ca. 750 Ma, see Li et al., 2008), or was located on the periphery of Rodinia (Zhou et al., 2006a,b; Wang et al., 2006), but not at a central Rodinia location as proposed by Z.X. Li et al. (1995). Most recently, Wang et al. (2007) studied the U–Pb ages of detrital zircon from the Lengjiaxi and Sibao Groups, and proposed that the Sibaoian orogenesis took place during the 860–800 Ma. It is noted, however, that the Lengjiaxi and Sibao Groups are nearly non-metamorphosed, in contrast to the Tianli Schist which were strongly deformed and metamorphosed to high greenschist facies during the Sibaorian orogenesis (Li et al., 2007a). In addition to the Mesoproterozoic and older zircons, the Neoproterozoic detrital zircons from Lengjiaxi and Sibao Groups display two major age peaks at ca. 890–940 Ma and ca. 850–865 Ma, which coincide with the ~ 900 Ma orogenic and ~ 850 Ma intraplate magmatic events in the SE Yangtze Block (Ye et al., 2007; Li et al., 2007c,e). Therefore, the Lengjiaxi and Sibao sedimentary rocks are unlikely to be related to the orogenesis, although their nature and the deposition environment need further investment.

The alternative viewpoint is that the Sibao orogeny occurred during ca. 1.1–0.9 Ga (Greentree et al., 2006; Li et al., 2006, 2007a; Ye et al., 2007), and the 830–740 Ma magmatic rocks were anorogenic products of mantle plume activities and continental rifting related to the breakup of Rodinia (e.g., Li et al., 1999, 2003a,b,c; Ling et al., 2003; Li et al., 2005; Zhu et al., 2006; Lin et al., 2007; Zhou et al., 2007). Recently, Li et al. (2007c) carried out a detailed geochronological and geochemical study of the Neoproterozoic magmatism in the eastern Yangtze Block. They suggested an upper age limit of ca. 0.9 Ga for the Sibaoian orogenesis based on the U–Pb zircon ages for the late-orogenic volcanic and granitoid rocks within the Shuangxiwu arc (Cheng, 1991, 1993; Ye et al., 2007), and the onset of the intraplate magmatism by ca. 850 Ma. There seems to be a magmatic quiescence between ca. 0.9 and ca. 0.85 Ga during which the tectonic regime transformed from Sibao orogenesis (Li et al., 2002a, 2006; Ye et al., 2007) to Nanhua rifting (Li, 1998; Wang and Li, 2003).

Identification of the ca. 880 Ma obduction-type leucogranites in the NE Jiangxi ophiolite sheds new lights on the tectonic evolution in South China. Obduction of the ca. 1.0 Ga NE Jiangxi ophiolite was related to the close of the back-arc basin during the waning stage of the collision between the Yangtze and Cathaysia Blocks (Li et al., 2002a). We note that the formation of ca. 880 Ma obduction-type leucogranites is consistent with not only the associated ca. 0.9 Ga high-pressure metamorphic blueschists (Charvet et al., 1996), but also the tectonic transformation from amalgamation to extension. Therefore, 880±19 Ma likely represents the terminal age of the tectonic convergence between the Yangtze and the Cathaysia Blocks in the Neoproterozoic.

6. Conclusion

High precision SHRIMP U–Pb zircon dating results indicate that the Xiwan leucogranite lenses were formed at 880 ± 19 Ma but was strongly overprinted by the Indosinian orogeny at ~ 230 Ma. Our detailed geochemical study shows that the Xiwan leucogranites have geochemistry characters similar to those of obduction-type granites within ophiolites, suggesting them being generated by partial melting of marginal basin sedimentary rocks beneath the obducting ophiolite. Three groups of leucogranites reflect variations in the depths of the partial melting. Identification of the ca. 880 ± 19 Ma obduction-type granites in the NE Jiangxi ophiolite allows us to constraint not only the timing of the ophiolite obduction probably related to the closing of the back-arc oceanic basin, but also the terminal age for the orogenesis between the Yangtze and Cathaysia Blocks during the assembly of Rodinia.

Acknowledgement

We appreciate the assistance of Y. Liu, X.L. Tu and X.R. Liang for geochemical and Nd isotopic analyses, and B. Song and H. Tao for SHRIMP U–Pb zircon analyses. H.Q. Fu, H.W. Zhou, J. Wang, S. Zhang and others are thanked for participating in, and discussions during, the various fieldtrips. The paper has benefited from review comments of Prof. Chan Wan Oh and an anonymous reviewer. This work was supported by NSFC (grants 40421303, 40573016), Chinese Academy of Sciences (grants KZCX3-SW-141 and 2003-2-1) and ARC Discovery Project grants (DP0450020 and DP0770228). This is TIGeR (The Institute of Geoscience Research) publication No. 100.

References

Ahmed, Z., 2003. Geochemical and genetic implications of adakites associated with the suprasubduction-type Al-Ays ophiolite, northwestern Arabian Shield. International Geology Review 45, 176–190.

Aldiss, D.T., 1981. Plagiogranites from the ocean crust and ophiolites. Nature 289, 577–578.

Black, L.P., Kamo, S.L., Allen, C.M., Aleinikoff, J.N., Davis, D.W., Korsch, R.J., Foudoulis, C., 2003. TEMORA 1: a new zircon standard for Phanerozoic U–Pb geochronology. Chemical Geology 200, 155–170.

Bureau of Geology and Mineral Resources of Jiangxi Province (BGMRJP), 1984. Regional Geology of Jiangxi Province. Geological Publishing House, Beijing. 921 pp.

Chappell, B.W., 1999. Aluminium saturation in I- and S-type granites and the characterization of fractionated haplogranites. Lithos 46, 535–551.

Charvet, J., Shu, L., Shi, Y., Guo, L., Faure, M., 1996. The building of south China: collision of Yangzi and Cathaysia blocks, problems and tentative answers. Journal of Southeast Asian Earth Sciences 13, 223–235.

Chen, J., Foland, K.A., Xing, F., Xu, X., Zhou, T., 1991. Magmatism along the southeastern margin of the Yangtze block: precambrian collision of the Yangtze and Cathysia blocks of China. Geology 19, 815–818.

Cheng, H., 1991. The late Proterozoic collision orogen in northwestern Zhejiang Province. Geology Reviews 3, 203–213 (in Chinese with English Abstract).

Cheng, H., 1993. Geochemistry of Proterozoic island-arc volcanic rocks in Northwest Zhejiang. Geochimica 1, 18–27 (in Chinese with English Abstract).

Coleman, R.G., 1977. Ophiolites. Springer-Verlag Berlin, Heidelberg, New York. 1–229 pp.

Coleman, R.G., Peterman, Z.E., 1975. Oceanic plagiogranite. Journal of Geophysical Research 80, 1099–1108.

Coleman, R.G., Donato, M.M., 1979. Oceanic plagiogranite revisited. In: Barker, F. (Ed.), Trondhjemites, Dacites, and Related Rocks. Elsevier Scientific Publishing Company Amsterdam, Oxford, New York, pp. 149–168.

Corfu, F., Hanchar, J.M., Hoskin, P.W.O., Kinny, P., 2003. Atlas of zircon textures. In: Hanchar, J.M., Hoskin, P.W.O. (Eds.), Zircon. Reviews in Mineralogy and Geochemistry, vol. 53. Mineralogical Society of America, pp. 468–500.

Cox, J., Searle, M., Pedersen, R., 1999. The petrogenesis of leucogranitic dykes intruding the northern Semail ophiolite, United Arab Emirates: field relationships, geochemistry and Sr/Nd isotope systematics. Contributions to Mineralogy and Petrology 137, 267–287.

Cumming, G.L., Richards, J.R., 1975. Ore lead isotope ratios in a continuously changing Earth. Earth and Planetary Science Letters 28, 155–171.

Dilek, Y., Furnes, H., Shallo, M., 2007. Suprasubduction zone ophiolite formation along the periphery of Mesozoic Gondwana. Gondwana Research 11, 453–475.

Dixon, S., Rutherford, M.J., 1979. Plagiogranites as late-stage immiscible liquids in ophiolite and mid-ocean ridge suits: an experimental study. Earth and Planetary Science Letters 45, 45–60.

Drummond, M.S., Defant, M.J., 1990. A model for trondhjemite-tonalite-dacite genesis and crustal growth via slab melting: archaean to modern comparisons. Journal of Geophysical Research 95, 21503–21521.

Elthon, D., 1991. Geochemical evidence for formation of the Bay of Islands ophiolite above a subduction zone. Nature 354, 140–143.

Flagler, P.A., Spray, J.G., 1991. Generation of plagiogranite by amphibolite anatexis in oceanic shear zones. Geology 19, 70–73.

Greentree, M.R., Li, Z.X., Li, X.H., Wu, H., 2006. Late Mesoproterozoic to earliest Neoproterozoic basin record of the Sibao orogenesis in western South China and relationship to the assembly of Rodinia. Precambrian Research 151, 79–110.

Hacker, B.P., 1994. Rapid emplacement of young oceanic lithosphere. Science 265, 1563–1565.

Hacker, B.P., Mosenfelder, J.L., Gnos, E., 1996. Rapid emplacement of the Oman Ophiolite: thermal and geochronologic constraints. Tectonics 15, 1230–1247.

Hu, A., Zhu, B., Mao, C., Zhu, N., Hunang, R., 1991. Geochronology of the Dahongshan Group. Chinese Journal of Geochemistry 10, 195–203.

Ishikawa, A., Kaneko, Y., Kadarusman, A., Ota, T., 2007. Multiple generations of forearc mafic–ultramafic rocks in the Timor–Tanimbar ophiolite, eastern Indonesia. Gondwana Research 11, 200–217.

Khan, M.S., Smith, T.E., Raza, M., Huang, J., 2007. Geology, geochemistry and tectonic significance of mafic–ultramafic rocks of Mesoproterozoic Phulad Ophiolite Suite of South Delhi Fold Belt, NW Indian Shield. Gondwana Research 8, 553–566.

Li, Z.X., Zhang, L., Powell, C.M., 1995. South China in Rodinia: part of the missing link between Australia–East Antarctica and Laurentia? Geology 23, 407–410.

Li, X.H., 1997. Timing of the Cathaysia Block formation: constraints from SHRIMP U–Pb zircon geochronology. Episodes 20, 188–192.

Li, X.H., Zhao, J.X., McCulloch, M.T., Zhou, G.Q., Xing, F.M., 1997. Geochemical and Sm–Nd isotopic study of Neoproterozoic ophiolites from southeastern China: petrogenesis and tectonic implications. Precambrian Research 81, 129–144.

Li, Z.X., 1998. Tectonic history of the major East Asian lithospheric blocks since the mid-Proterozoic — a synthesis. AGU Geodynamics Series, v. 27, Washington, DC, pp. 221–243.

Li, X.H., 1999. U–Pb zircon ages of granites from the southern margin of the Yangtze Block: timing of Neoproterozoic Jinning: Orogeny in SE China and implications for Rodinia Assembly. Precambrian Research 97, 43–57.

Li, Z.X., Li, X.H., Kinny, P.D., Wang, J., 1999. The breakup of Rodinia: did it start with a mantle plume beneath South China? Earth and Planetary Science Letters 173, 171–181.

Li, X.H., Sun, M., Wei, G.J., Liu, Y., Lee, C.Y., Malpas, J.G., 2000. Geochemical and Sm–Nd isotopic study of amphibolites in the Cathaysia Block, SE China: evidence for extremely depleted mantle in the Paleoproterozoic. Precambrian Research 102, 251–262.

Li, Z.X., Li, X.H., Zhou, H.W., Kinny, P.D., 2002a. Grenvillian continental collision in south China: New SHRIMP U–Pb zircon results and implications for the configuration of Rodinia. Geology 30, 163–166.

Li, X.H., Liu, Y., Tu, X.L., Hu, G.Q., Zeng, W., 2002b. Precise determination of chemical compositions in silicate rocks using ICP-AES and ICP-MS: a comparative study of sample digestion techniques of alkali fusion and acid dissolution. Geochimica 31, 289–294 (in Chinese with English abstract).

Li, X.H., Li, Z.X., Zhou, H., Liu, Y., Kinny, P.D., 2002c. U–Pb zircon geochronology, geochemistry and Nd isotopic study of Neoproterozoic bimodal volcanic rocks in the Kangdian Rift of South China: implications for the initial rifting of Rodinia. Precambrian Research 113, 135–154.

Li, W.X., Li, X.H., 2003. Adakitic granites within the NE Jiangxi ophiolites, South China: geochemical and Nd isotopic evidence. Precambrian Research 122, 20–44.

Li, Z.X., Wang, J., Li, X.H., Zhang, S.H., 2003a. From Sibao Orogenesis to Nanhua Rifting: Late Precambrian Tectonic History of Eastern South China. Geological Publishing House, Beijing. 100 pp.

Li, X.H., Li, Z.X., Ge, W., Zhou, H., Li, W., Liu, Y., Wingate, M.T.D., 2003b. Neoproterozoic granitoids in South China: crustal melting above a mantle plume at 825 Ma? Precambrian Research 122, 45–83.

Li, Z.X., Li, X.H., Kinny, P.D., Wang, J., Zhang, S., Zhou, H., 2003c. Geochronology of Neoproterozoic syn-rift magmatism in the Yangtze Craton, South China and correlations with other continents: evidence for a mantle superplume that broke up Rodinia. Precambrian Research 122, 85–109.

Li, X.H., Liu, D.Y., Sun, M., Li, W.X., Liang, X.R., Liu, Y., 2004. Precise Sm–Nd and U–Pb isotopic dating of the super-giant Shizhuyuan polymetallic deposit and its host granite, Southeast China. Geological Magazine 141, 225–231.

Li, W.X., Li, X.H., Li, Z.X., 2005. Neoproterozoic bimodal magmatism in the Cathaysia Block of South China and its tectonic significance. Precambrian Research 136, 51–66.

Li, X.H., Li, Z.X., Sinclair, J.A., Li, W.X., Carter, G., 2006. Revisiting the Yanbian Terrane: implications for Neoproterozoic tectonic evolution of the western Yangtze Block, South China. Precambrian Research 151, 14–30.

Li, Z.X., Wartho, J.A., Occhipinti, S., Zhang, C.L., Li, X.H., Wang, J., Bao, C., 2007a. Early history of the eastern Sibao orogen (South China) during the assembly of Rodinia: new $^{40}Ar/^{39}Ar$ dating and U–Pb SHRIMP detrital zircon provenance constraints. Precambrian Research 159, 74–94.

Li, Z.X., Li, X.H., 2007b. Formation of the 1300-km-wide intracontinental orogen and postorogenic magmatic province in Mesozoic South China: a flat-slab subduction model. Geology 35, 179–182.

Li, X.H., Li, W.X., Li, Z.X., Liu, Y., 2007c. 850–790 Ma bimodal volcanic and intrusive rocks in northern Zhejiang, South China: a major episode of continental rift magmatism during the breakup of Rodinia. Lithos. doi:10.1016/j.lithos.2007.04.007.

Li, X.H., Li, W.X., Li, Z.X., 2007d. On the genetic classifications and tectonic implications of the Early Yanshanian granitoids in the Nanling Range of South China. Chinese Science Bulletin 52, 1873–1885.

Li, X.H., Li, W.X., Li, Z.X., 2007e. Ca. 850 Ma intraplate magmatism in South China: implications for onset of the breakup of Rodinia. Geochimica et Cosmochimica Acta 71, A575.

Li, Z.X., Bogdanova, S.V., Collins, A.S., Davidson, A., De Waele, B., Ernst, R.E., Fitzsimons, I.C.W., Fuck, R.A., Gladkochub, D.P., Jacobs, J., Karlstrom, K.E., Lu, S., Natapov, L.M., Pease, V., Pisarevsky, S.A., Thrane, K., Vernikovsky, V., 2008. Assembly, configuration, and break-up history of Rodinia: a synthesis. Precambrian Research 160, 179–210.

Lin, G.C., Li, X.H., Li, W.X., 2007. SHRIMP U–Pb zircon age, geochemistry and Nd–Hf isotope of Neoproterozoic mafic dyke swarms in western Sichuan: petrogenesis and tectonic significance. Science in China. Series D 50, 1–16.

Ling, W., Gao, S., Zhang, B., Li, H., Liu, Y., Cheng, J., 2003. Neoproterozoic tectonic evolution of the northwestern Yangtze Craton, South China: implications for amalgamation and break-up of the Rodinia Supercontinent. Precambrian Research 122, 111–140.

Liu, D., Jian, P., Zhang, Q., Zhang, F., Shi, Y., Shi, G., Zhang, N., Tao, H., 2003. SHRIMP dating of adakites in the Yulingkai ophiolite, Inner Mongolia: evidence for the Early Paleozoic subduction. Acta Geologica Sinica 77, 317–327 (in Chinese with English abstract).

Patiño Douce, A.E., Harris, N., 1998. Experimental constraint on Himalayan anatexis. Journal of Petrology 39, 689–710.

Patiño Douce, A.E., McCarthy, T.C., 1998. Melting of crustal rocks during continental collision and subduction. In: Harker, B.R., Liu, J.G. (Eds.), When Continents Collide: Geodynamics and Geochemistry of Ultrahigh-Pressure Rocks. Kluwer Academic Publishers, pp. 27–55.

Pearce, J.A., 1989. High T/P metamorphism and granite genesis beneath ophiolite thrust sheets. Ophioliti 14, 195–211.

Pearce, J.A., Harris, N.B.W., Tindle, A.G., 1984. Trace element discrimination diagrams for the tectonic interpretation of granitic rocks. Journal of Petrology 25, 956–983.

Pedersen, R.B., Malpas, J., 1984. The origin of oceanic plagiogranites from the Karmoy ophiolite, Western Norway. Contributions to Mineralogy and Petrology 88, 36–52.

Peter, T., Kamber, B.S., 1994. Peraluminous, potassium-rich granitoids in the Semail Ophiolite. Contributions to Mineralogy and Petrology 118, 229–238.

Qiu, Y.M., Gao, S., McNaughton, N.J., Groves, D.I., Ling, W., 2000. First evidence of >3.2 Ga continental crust in the Yangtze Craton of South China and its implications for Archean Crustal Evolution and Phanerozoic Tectonics. Geology 28, 11–14.

Shu, L., Zhou, G., Shi, Y., Ying, J., 1994. Study of the high-pressure metamorphic blueschist and its late Proterozoic age in the eastern Jiangnan orogeny belt. Chinese Science Bulletin 39, 1200–1204.

Skjerlie, K.P., Pedersen, R.B., Wennberg, O.P., De La Rosa, J., 2000. Volatile phase fluxed anatexis of sediments during late Caledonian ophiolite obduction: evidence from the Sogneskollen granitic complex, west Norway. Journal of the Geological Society of London 157, 1199–1213.

Sorenson, S.S., Grossman, J.N., 1989. Enrichment of trace elements in garnet amphibolites from a paleo-subduction zone: Catalina Schist, southern California. Geochimica et Cosmochimica Acta 53, 3155–3177.

Sun, S.S., McDonough, W.F., 1989. Chemical and isotopic systematics of oceanic basalt: implication for mantle composition and process. In: Sauders, A.D., Norry, M.J. (Eds.), Magmatism in the Ocean Basin: Geological Society of London Special Publication, vol .42, pp. 313–345.

Tanaka, T., 19 co-authors, 2000. JNdi-1: a neodymium isotopic reference in consistency with LaJolla neodymium. Chemical Geology 168, 279–281.

Wang, J., Li, Z.X., 2003. History of Neoproterozoic rift basins in South China: implications for Rodinia break-up. Precambrian Research 122, 141–158.

Wang, X.L., Zhou, J.C., Qiu, J.S., Gao, J.F., 2004. Geochemistry of the Meso- to Neoproterozoic basic-acid rocks from Hunan Province, South China: implications for the evolution of the western Jiangnan orogen. Precambrian Research 135, 79–103.

Wang, X.L., Zhou, J.C., Qiu, J.S., Zhang, W.L., Liu, X.M., Zhang, G.L., 2006. LA-ICP-MS U–Pb zircon geochronology of the Neoproterozoic igneous rocks from Northern Guangxi, South China: Implications for tectonic evolution. Precambrian Research 145, 111–130.

Wang, X.L., Zhou, J.C., Griffin, W.L., Wang, R.C., Qiu, J.S., O'Reilly, S.Y., Xu, X.S., Liu, X.M., Zhang, G.L., 2007. Detrital zircon geochronology of Precambrian basement sequences in the Jiangnan orogen: dating the assembly of the Yangtze and Cathaysia blocks. Precambrian Research 159, 117–131.

Whitehead, J., Dunning, G.R., Spray, J.G., 2000. U–Pb geochronology and origin of granitoid rocks in the Thetford Mines ophiolite, Canadian Appalachians. GSA Bulletin 112, 915–928.

Williams, I.S., 1998. U–Th–Pb geochronology by ion microprobe. Applications of microanalytical techniques to understanding mineralizing processes. Reviews in Economic Geology 7, 1–35.

Wu, R.X., Zheng, Y.F., Wu, Y.B., Zhao, Z.F., Zhang, S.B., Liu, X.M., Wu, F.Y., 2006. Reworking of juvenile crust: element and isotope evidence from Neoproterozoic granodiorite in South China. Precambrian Research 146, 179–212.

Ye, M.F., Li, X.H., Li, W.X., Liu, Y., Li, Z.X., 2007. SHRIMP zircon U–Pb geochronological and whole-rock geochemical evidence for an early Neoproterozoic Sibaoan magmatic arc along the southeastern margin of the Yangtze Block. Gondwana Research 12, 144–156.

Yoshikawa, M., Ozawa, K., 2007. Rb–Sr and Sm–Nd isotopic systematics of the Hayachine–Miyamori ophiolitic complex: melt generation process in the

mantle wedge beneath an Ordovician island arc. Gondwana Research 11, 234–246.

Zhang, S.B., Zheng, Y.F., Wu, Y.B., Zhao, Z.F., Gao, S., Wu, F.Y., 2006. Zircon isotope evidence for >3.5 Ga continental crust in the Yangtze craton of China. Precambrian Research 146, 16–34.

Zhou, G.Q., 1989. The discovery and significance of the northeastern Jiangxi Province ophiolite (NEJXO), its metamorphic peridotite and associated high temperature-high pressure metamorphic rocks. Journal of Southeast Asian Earth Sciences 3, 237–247.

Zhou, G.Q., 1997. Jadeitic rocks from high-pressure metamorphic zone of NE Jiangxi province: formation and preservation condition. Science in China. Series D 27, 45–51 (in Chinese with English abstract).

Zhou, M.F., Yan, D.P., Kennedy, A.K., Li, Y., Ding, J., 2002a. SHRIMP U–Pb zircon geochronological and geochemical evidence for Neoproterozoic arc-magmatism along the western margin of the Yangtze Block, South China. Earth and Planetary Science Letters 196, 51–67.

Zhou, M.F., Kennedy, A.K., Sun, M., Malpas, J., Lesher, C.M., 2002b. Neoproterozoic arc-related mafic intrusions along the northern margin of South China: implications for the accretion of Rodinia. Journal of Geology 110, 611–618.

Zhou, M.F., Ma, Y., Yan, D.P., Xia, X., Zhao, J.H., Sun, M., 2006a. The Yanbian Terrane (Southern Sichuan Province, SW China): a Neoproterozoic arc assemblage in the western margin of the Yangtze Block. Precambrian Research 144, 19–38.

Zhou, M.F., Yan, D.P., Wang, C.L., Xia, X., Zhao, J.H., Sun, M., 2006b. Subduction-related origin of the 750 Ma Xuelongbao adakitic complex (Sichuan Province, China): implications for the tectonic setting of the giant Neoproterozoic magmatic event in South China. Earth and Planetary Science Letters 248, 286–300.

Zhou, J.B., Li, X.H., Ge, W., Li, Z.X., 2007. Age and origin of middle Neoproterozoic mafic magmatism in southern Yangtze Block and relevance to the break-up of Rodinia. Gondwana Research 12, 184–197.

Zhu, W.G., Zhong, H., Deng, H.L., Wilson, A.H., Liu, B.G., Li, C.Y., 2006. SHRIMP zircon U–Pb age, geochemistry and Nd–Sr isotopes of the Gaojiacun mafic–ultramafic intrusive complex, SW China. International Geology Review 48, 650–668.

Zoheir, B.A., Klemm, D.D., 2007. The tectono-metamorphic evolution of the central part of the Neoproterozoic Allaqi–Heiani suture, south Eastern Desert of Egypt. Gondwana Research 12, 289–304.